ACS OMEGA

http://pubs.acs.org/journal/acsodf

Article

Gallium-68 Labeling of the Cyclin-Dependent Kinase 4/6 Inhibitors as Positron Emission Tomography Radiotracers for Tumor Imaging

Cheng Liu,[#] Ziyi Yang,[#] Mingyu Liu, Xiangwei Wang, Shaoli Song,* Xiaoping Xu,* and Zhongyi Yang*

Cite This: *ACS Omega* 2021, 6, 32253−32261

Read Online

ACCESS | Metrics & More | Article Recommendations

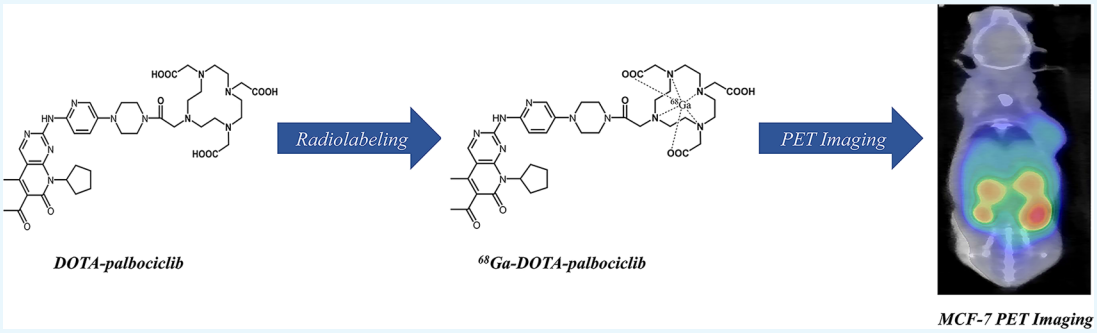

ABSTRACT: Cyclin-dependent kinase 4 and 6 (CDK4/6) have emerged as interesting therapeutic drug targets with many potential applications in anti-tumors, especially in breast cancer. A novel CDK4/6 kinase-derived positron emission tomography (PET) imaging agent was designed based on palbociclib modified with a chelator DOTA. This new compound with a chelator DOTA-palbociclib was radiolabeled with gallium 68 (^{68}Ga). After labeling, the purity and stability were evaluated, and the blood pharmacokinetics were carried out in normal healthy mice. Human breast cancer MCF-7 (ER+/HER2−) cells were used for *in vitro* cell uptake tests. PET imaging and *ex vivo* biodistribution were conducted in MCF-7 tumor-bearing mice. Specific binding of tumors was evaluated by the blocking assay. Furthermore, the uptake of ^{68}Ga-DOTA-palbociclib in tumors was studied by autoradiography of tissue sections followed by immunofluorescence evaluation of CDK4 and CDK6. ^{68}Ga-DOTA-palbociclib was synthesized very simply in a high labeling rate and radiochemical purity in 10 min. The labeling compound showed excellent stability both *in vitro* and *in vivo* and exhibited good pharmacokinetics, making it suitable for *in vivo* imaging. Cell uptake studies display that co-incubation with palbociclib can inhibit cellular uptake of ^{68}Ga-DOTA-palbociclib. *In vivo* imaging and *ex vivo* biodistribution in mice bearing MCF-7 tumors both showed obvious radioactive uptake in the tumor and higher tumor-to-muscle ratios, while the tumor radioactivity accumulation was significantly decreased when prior administered with an excess of cold palbociclib, confirming CDK4/6 specific binding of ^{68}Ga-DOTA-palbociclib *in vivo*. Autoradiography of the avid tumor section showed a high correlation between immunofluorescence with the CDK4/6 positive areas of the tumor, further demonstrating that ^{68}Ga-DOTA-palbociclib specifically targeted CDK4/6 positive tumors. We synthesized ^{68}Ga-DOTA-palbociclib, a new CDK4/6 kinase PET imaging agent, and validated its excellent stability, pharmacokinetics, and specific tumor binding. Based on our primary results, ^{68}Ga-DOTA-palbociclib is a promising imaging agent with the potential to tailor a precise treatment program for CDK4/6 inhibitors.

INTRODUCTION

The mammalian cell cycle is a sequence of events essential for cellular reproduction and function, which contains four distinct phases (G1, S, G2, and M).[1] Cell cycle control is frequently disrupted in most cancers,[2,3] and research on it has become a new attractive target for novel cancer therapeutics. Cyclin-dependent kinase 4 and 6 (CDK4/6) are fundamental drivers of the cell cycle.[4] Once activated and after binding with cyclin D, CDK4/6 phosphorylates the retinoblastoma protein (Rb), an event that causes Rb to lose the ability to bind to the E2F family of transcription factors, and thus helps to drive the progression from the G1 to S phase of cells.[5] Amplification and overexpression of the CDK4/6 and cyclin D have been found to exist in a variety of malignancies including breast cancer.[6,7] As noted above, inhibiting CDK4 and CDK6 prevents cell cycle progression, suppressing tumor development and promoting senescence. Thus, the development of selective CDK4/6 inhibitors has become a novel therapeutic frontier for patients with advanced cancer.

Received: September 13, 2021
Accepted: November 5, 2021
Published: November 18, 2021

https://doi.org/10.1021/acsomega.1c05073
ACS Omega 2021, 6, 32253−32261

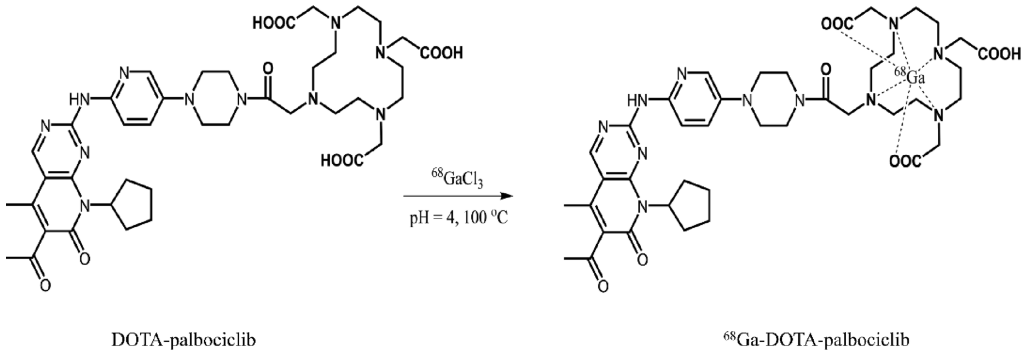

Figure 1. Structure and synthesis scheme for ^{68}Ga-DOTA-palbociclib.

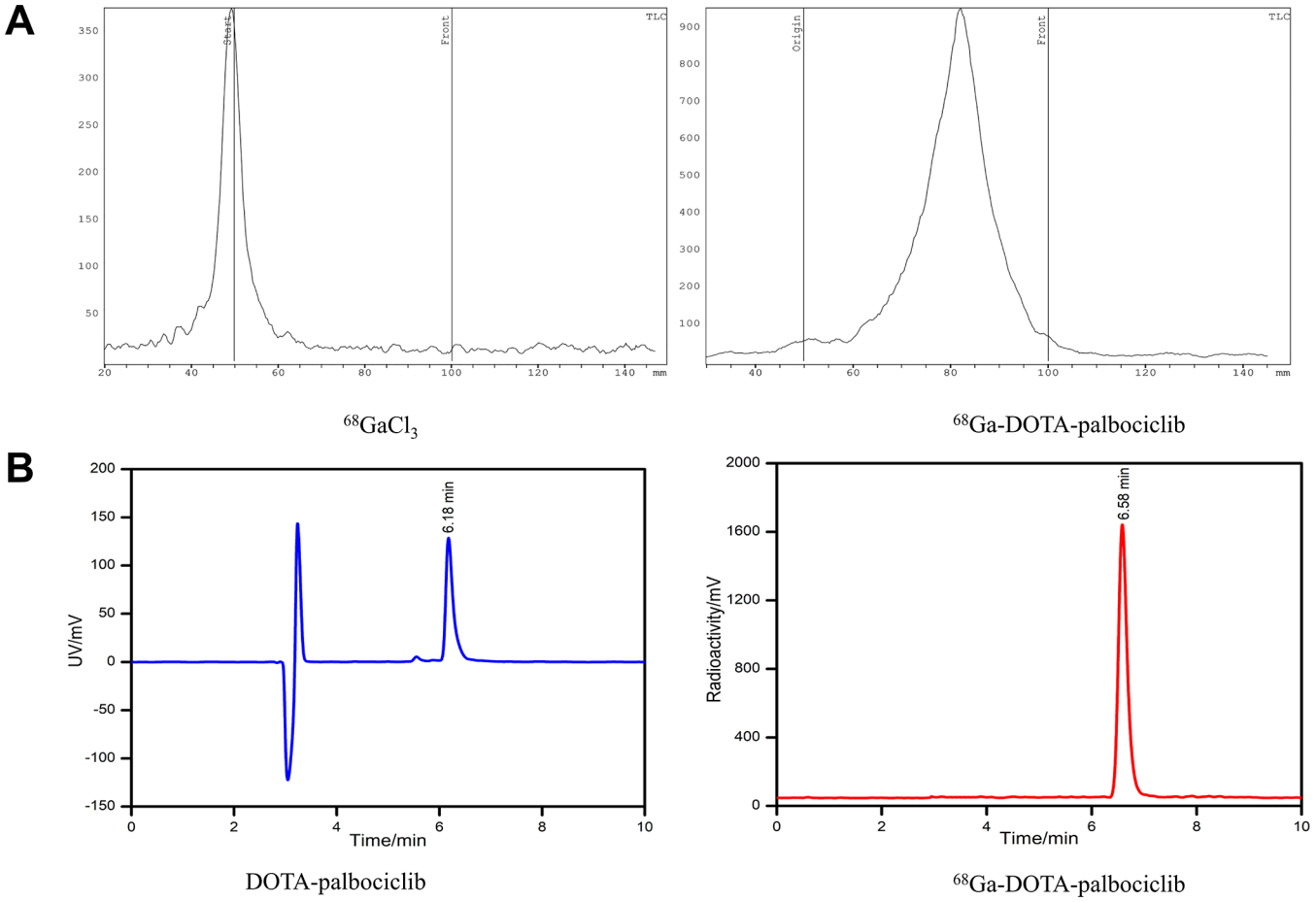

Figure 2. Quality control of ^{68}Ga-DOTA-palbociclib. (A) Typical radio-TLC chromatograms of $^{68}GaCl_3$ (left) and ^{68}Ga-DOTA-palbociclib (right). (B) Typical HPLC chromatograms of DOTA-palbociclib (left) and ^{68}Ga-DOTA-palbociclib (right).

To date, three selective CDK4/6 inhibitors, palbociclib, ribociclib, and abemaciclib, have been approved for the treatment of hormone receptor (HR)-positive, human epidermal growth factor receptor 2 (HER2)-negative breast cancer. A large number of clinical trials have demonstrated that the combination of CDK4/6 inhibitors and endocrine therapy significantly improved clinical outcomes, such as extending the progression-free survival (PFS) and overall survival (OS) in HR-positive metastatic breast cancer.[8−11] Despite the prominent benefit of this combination, some patients might show de novo resistance to CDK4/6 inhibitors, and nearly all patients will eventually acquire resistance to these drugs.[12,13] Therefore, the early identification of patients who will benefit from CDK4/6 inhibitors is very important. The early prediction will avoid treatment-related toxicity and can lead to improving patient survival by allowing early intensive treatment.

CDK4/6 expression is routinely determined by the invasive method of immunohistochemistry (IHC) at the time of diagnosis of the primary tumor. Furthermore, the role of IHC is limited in analyzing the heterogeneity of CDK4/6 expression in primary tumors and the heterogeneity of CDK4/6 expression between primary and metastatic lesions. In contrast, noninvasive molecular imaging provides a potentially valuable approach for visualization of CDK4/6 positive lesions and quantification of CDK4/6 expression *in vivo*, including the metastasis that cannot be a biopsy.

https://doi.org/10.1021/acsomega.1c05073
ACS Omega 2021, 6, 32253−32261

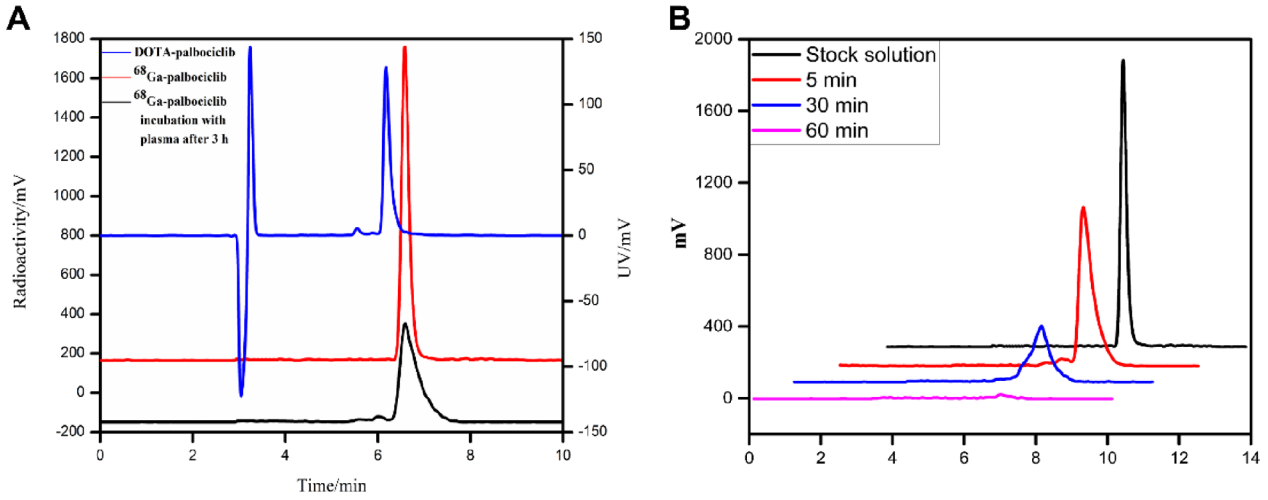

Figure 3. *In vitro* and *in vivo* stability. (A) Typical HPLC chromatograms of DOTA-palbociclib (blue line), ^{68}Ga-DOTA-palbociclib (red line), and ^{68}Ga-DOTA-palbociclib incubation with fresh mouse plasma after 3 h (black line). (B) Typical radio-HPLC chromatograms of ^{68}Ga-DOTA-palbociclib in saline before injection and in the plasma at 5, 30, and 60 min p.i.

Gallium 68 is a metal positron emitter, an isotope used for positron emission tomography (PET) imaging produced by a ^{68}Ge/^{68}Ga generator. ^{68}Ga, with a suitable half-life (68 min) and simple labeling condition, is an ideal radionuclide for developing a new molecular probe based on targeted drugs. With the commercialization and universalization of the ^{68}Ge/^{68}Ga generator, ^{68}Ga-labeled radiopharmaceuticals have displayed a good application prospect in PET imaging and can be seen as a scheme of alternatives to cyclotron-produced PET isotopes, such as ^{18}F.[14−16]

The goal of the current study was to develop a novel PET tracer (^{68}Ga-DOTA-palbociclib) for imaging of CDK4/6 *in vivo*. We outline the synthesis and the radiochemical and biological properties of ^{68}Ga-DOTA-palbociclib involved in cellular uptake studies, metabolism, and biodistribution studies and explore its potential for PET imaging. Both *in vitro* and *in vivo* studies were performed in MCF7 breast carcinoma cells, and subcutaneous xenografts were derived from this cell line, a molecular subtype of HR+/HER2− breast cancer.

RESULTS

Radiolabeling and Octanol−Water Partition Coefficient. Figure 1 shows the structure and synthesis scheme for ^{68}Ga-DOTA-palbociclib. Using the iTLC-SG, the radiochemical purity (RCP) of ^{68}Ga-DOTA-palbociclib could be obtained in 5 min. The R_f of ^{68}Ga-DOTA-palbociclib was 0.6−0.7, and the R_f of $^{68}GaCl_3$ was 0−0.1. As displayed in Figure 2, the radiochemical purity of ^{68}Ga-DOTA-palbociclib was >95%. Furthermore, radio-HPLC confirmed the ^{68}Ga-DOTA-palbociclib and its RCP. The retention time of DOTA-palbociclib (UV peak) was 6.18 min, and the retention time of ^{68}Ga-DOTA-palbociclib (radioactive peak) was 6.58 min. The proximity in retention time demonstrated that the Ga-68 had radiolabeled DOTA-palbociclib successfully. The radio-HPLC spectrum confirmed the high RCP of ^{68}Ga-DOTA-palbociclib (>95%). The log $P_{octanol/water}$ value was −1.64 ± 0.12, revealing that ^{68}Ga-DOTA-palbociclib was more hydrophilic than palbociclib.

***In Vitro* and *In Vivo* Stability.** First of all, the stability of ^{68}Ga-DOTA-palbociclib was measured in PBS (0.1 M pH = 7.4). ^{68}Ga-DOTA-palbociclib was stable in PBS for 3 h, and no free Ga-68 was found by radio-TLC. To better mimic the complex internal environment, fresh mouse plasma was used to evaluate the stability of ^{68}Ga-DOTA-palbociclib. After 3 h of incubation and protein precipitation, the supernatant of plasma was analyzed by radio-HPLC. The result is illustrated in Figure 3A. The peak time of the sample was consistent with the retention time of ^{68}Ga-DOTA-palbociclib, and no other obvious peak was found. These results demonstrated that ^{68}Ga-DOTA-palbociclib remained prototype in plasma for 3 h, and there was not any degradation. All in all, ^{68}Ga-DOTA-palbociclib was very stable *in vitro*.

Since all the imaging probes will be used *in vivo* ultimately, it is necessary to determine the *in vivo* stability of ^{68}Ga-DOTA-palbociclib. After intravenous injection of ^{68}Ga-DOTA-palbociclib, the mice were killed with painless bleeding under anesthesia at 5, 30, and 60 min. The blood was collected and mixed with acetonitrile for protein precipitation. The supernatant was also analyzed by radio-HPLC, and the result is displayed in Figure 3B. There was only one peak in the radioactive chromatograms of the supernatant collected from the blood sample at 5 or 30 min after ^{68}Ga-DOTA-palbociclib injection. Although the analysis result of blood collected at 60 min after injection showed that the radioactivity was very low, no other obvious peak was observed in the HPLC chromatogram. By comparison with the chromatogram of ^{68}Ga-DOTA-palbociclib, it was proven that the peak of the blood sample at 5, 30, or 60 min represented ^{68}Ga-DOTA-palbociclib. As a consequence, it could be considered that ^{68}Ga-DOTA-palbociclib displayed high stability *in vivo*.

Cell Uptake and Pharmacokinetics. *In vitro* binding of ^{68}Ga-DOTA-palbociclib to CDK4/6 on MCF-7 cells was investigated using the cell uptake assay. In the presence of an excess of unlabeled palbociclib, cell uptake could be blocked by approximately 86% (Figure 4A, $P < 0.001$). The radioactivity in mouse blood shows that the ^{68}Ga-DOTA-palbociclib cleared relatively fast *in vivo*. The distribution phase half-life t1/2α of ^{68}Ga-DOTA-palbociclib was estimated to be 4.30 min, and the clear-phase half-life t1/2β was estimated to be 69.315 min (Figure 4B).

^{68}Ga-DOTA-Palbociclib PET/CT Imaging. The PET/CT images were obtained for ^{68}Ga-DOTA-palbociclib in MCF-7

https://doi.org/10.1021/acsomega.1c05073
ACS Omega 2021, 6, 32253−32261

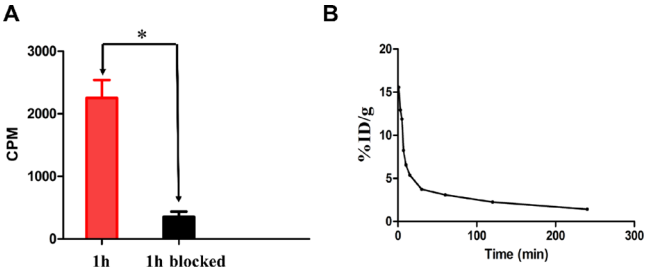

Figure 4. Cell uptake and pharmacokinetics. (A) *In vitro* uptake by MCF-7 cells incubated with ^{68}Ga-DOTA-palbociclib in the absence (red column) or presence (black column) of an excess of unlabeled palbociclib after 1 h (*P < 0.001). (B) Blood pharmacokinetics of ^{68}Ga-DOTA-palbociclib in healthy mice ($t1/2_{\alpha}$ = 4.30 min, $t1/2_{\beta}$ = 69.31 5 min).

tumor-bearing mice at 1 h after injection. As shown in Figure 5A, there was a high radioactivity accumulation in the tumor. The specificity of ^{68}Ga-DOTA-palbociclib for CDK4/6 was again confirmed by the blocking experiment. The tumor uptake was almost completely decreased to the background level in the mouse pretreated with excessive cold palbociclib, which was a statistically significant difference compared with that in the unblocked mice (Figure 4B, 0.63 ± 0.05 vs 0.21 ± 0.05 SUV, P = 0.002). Consistent with the above results, there is a significant statistical difference in T/M between the blocked group and the unblocked group (Figure 4C, 3.72 ± 0.47 vs 1.26 ± 0.22, P < 0.001). Equally notable is that the PET images showed obvious abdominal uptake.

***Ex Vivo* Biodistribution, Autoradiography, and Immunofluorescence.** The *in vivo* tumor targeting and imaging features of ^{68}Ga-DOTA-palbociclib were further evaluated by an *ex vivo* biodistribution study (Figure 6). There was a high (4.07 ± 0.18% ID/g) accumulation of the radioactivity in the

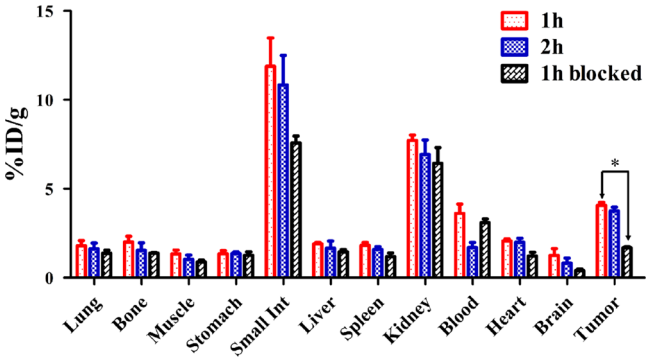

Figure 6. ^{68}Ga-DOTA-palbociclib *ex vivo* biodistribution in MCF-7 tumor-bearing mice (n = 3 per group), at 1 h (red bar) and 2 h (blue bar) post-injection or with a pre-injection excess of palbociclib blocking (black bar), here expressed as %ID/g.

tumors at 1 h post-injection. At the time points of 2 h post-injection, the uptake of the radiotracer in the tumor was slightly decreased (3.75 ± 0.22% ID/g), but there is no significant difference compared with 1 h points (P = 0.193). It is worth noting that high normal tissue radioactivities were observed in the small intestine (11.89 ± 1.58 or 10.84 ± 1.66% ID/g) and kidney (7.72 ± 0.31 or 6.93 ± 0.81% ID/g) at 1 or 2 h after injection. High uptake of the small intestine may be one of the causes for the marked abdominal accumulated in the PET image.

To evaluate the specificity of ^{68}Ga-DOTA-palbociclib binding to CDK4/6, a group of MCF-7 tumor-bearing mice

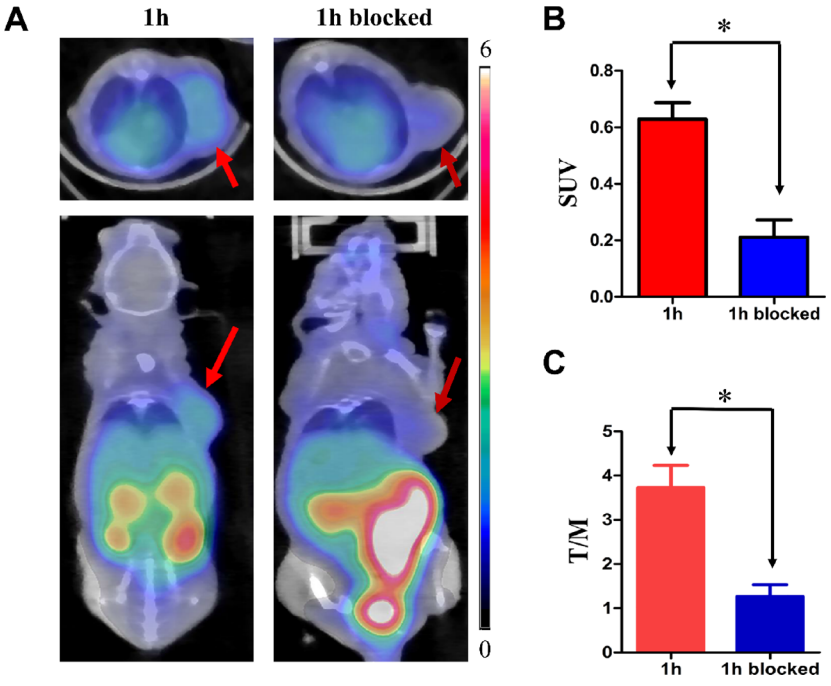

Figure 5. *In vivo* small-animal PET/CT images and quantitative analysis parameters. (A) Representative MicroPET/CT images of ^{68}Ga-DOTA-palbociclib in MCF-7 tumor xenografts *in vivo*. Transverse and coronal images at 1 h after injection (without an excess of palbociclib, left; with an excess of palbociclib 30 min before ^{68}Ga-DOTA-palbociclib, right; red arrows point to tumor tissues). (B) Significance of tumor SUV between ^{68}Ga-DOTA-palbociclib and the blocked group. (C) The ratio of the tumor to the contralateral muscle was analyzed in the ^{68}Ga-DOTA-palbociclib image. *P < 0.05.

https://doi.org/10.1021/acsomega.1c05073
ACS Omega 2021, 6, 32253−32261

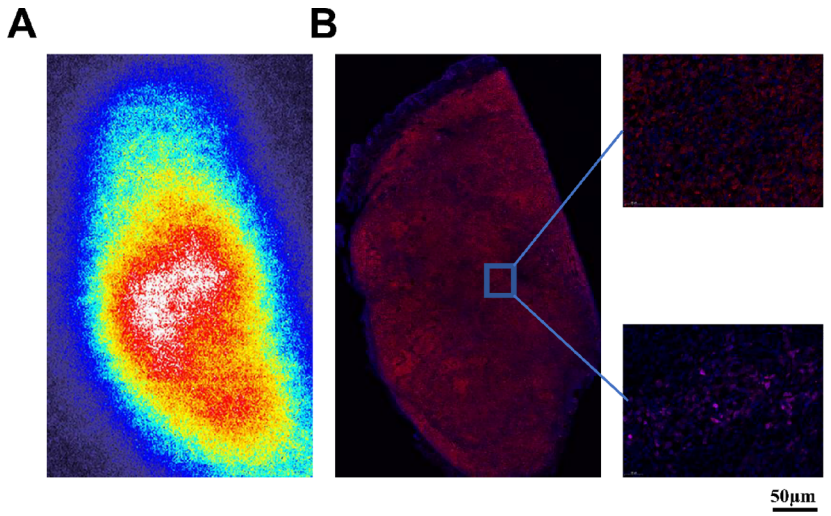

Figure 7. Autoradiography and immunofluorescence. (A) Autoradiography image showing distribution of radioactivity. (B) Immunofluorescence image showing CDK4 (red), CDK6 (pink), and nuclei (blue).

(n = 3) was injected with an excess of palbociclib 30 min prior to receiving ^{68}Ga-DOTA-palbociclib (at 1 h point). In the blocking group, the tumor uptake was decreased to 1.67 ± 0.07% ID/g, which was remarkably different from the unblocked group (P = 0.001).

To further investigate the correlation between the protein of CDK4/6 expression and radioactive uptake, we performed ^{68}Ga-DOTA-palbociclib autoradiography and immunofluorescence staining in adjacent sections. As shown in autoradiography images (Figure 7A), the ^{68}Ga-DOTA-palbociclib signal was visibly accumulated in the tumor and consistent with paralleled immunofluorescence for the positive staining of CDK4 and CDK6 in the tumor (Figure 7B). Consequently, we demonstrated that ^{68}Ga-DOTA-palbociclib was specifically bound to CDK4 and CDK6 positive tumors.

DISCUSSION

Here, we elaborate on the use of ^{68}Ga-DOTA-palbociclib PET to perform non-invasive imaging of CDK4/6, which is the key regulator of the cell cycle process by regulating the G1-S checkpoint. Palbociclib is the first oral CDK4/6 inhibitor approved by the FDA and currently the most widely used CDK4/6 inhibitor in the world, including China.[17] Therefore, the palbociclib analogue was selected as the precursor to synthesize targeted CDK4/6 radiopharmaceutical agents.

In the clinical practice aspect, the application of CDK4/6 inhibitors on breast cancer becomes broader and broader; therefore, it is of great significance to further understand the mechanisms of resistance and potential biomarkers of CDK4/6 inhibitors.[18,19] However, it is well known that many potential drug resistance mechanisms have been identified in preclinical studies but cannot be further confirmed in real clinical trials.[20−22] In view of this, we synthesized ^{68}Ga-DOTA-palbociclib to monitor the expression of CDK4/6 in tumors or other tissues as a valuable method for predicting which patients will respond to CDK4/6 inhibitor therapy. In addition, we combined multiple molecular imaging technologies, such as ^{18}F-FES[23] or ^{18}F-FLT,[24] to evaluate the target engagement and early therapeutic efficacy of CDK4/6 inhibitors combined with endocrine therapy. Finally, serial ^{68}Ga-DOTA-palbociclib imaging can be used to study the pharmacokinetics of palbociclib by evaluating the residual availability of CDK4/6 on tumors during palbociclib treatment and therefore has the potential to assist in the design of an optimum therapeutic regimen.

To our knowledge, this is the first report on CDK4/6 imaging using Ga-68 labeling palbociclib analogues. The earliest reports on CDK4 imaging radiotracers were ^{124}I-CKIA and ^{124}I-CKIB.[25] Unfortunately, these tracers showed no radioactivity accumulation *in vivo* xenografts in small-animal PET imaging, and there is only a slight uptake in *ex vivo* autoradiography. Recently, Song et al.[26,27] provided a proof of concept that palbociclib labeled with ^{99m}Tc was a potential tracer for CDK4/6 detection by SPECT. Consistent with the results of Gan et al.,[27] the blood uptake of ^{68}Ga-DOTA-palbociclib was higher at 1 h after injection, but it was quickly cleared and decreased by about 54% at 2 h after injection (from 3.61 ± 0.53 to 1.69 ± 0.29% ID/g). The most important difference is that the MCF-7 tumor uptake of ^{68}Ga-DOTA-palbociclib was significantly higher than that of blood after 2 h of injection (3.75 ± 0.22% vs 1.69 ± 0.29% ID/g), while the uptake of ^{99m}Tc-labeled tracers was still lower than that of blood, indicating that ^{68}Ga-DOTA-palbociclib possessed better imaging to CDK4/6. However, compared with the ^{18}F-CDKi studied by Ramos et al.,[28] the tumor-blood ratio of ^{68}Ga-DOTA-palbociclib seems unsatisfactory, and the development of radiotracers with lower blood retention might be the main focus of a subsequent study. Furthermore, PET imaging tracers may improve the characteristics of small lesions due to the higher spatial resolution of clinical PET imaging than SPECT imaging tracers and provide a reliable quantitative method for evaluating the uptake of radiotracers by tumors and normal organs.[29] In this context, Ramos et al. synthesized ^{18}F-CDKi to represent the PET imaging tracer to monitor against CDK4/6 kinases.[28] Although ^{18}F-CDKi is a promising imaging agent, the application of ^{18}F requires a cyclotron on-site and the cumbersome synthesis method limits it further in a clinical setting in certain aspects. According to the report,[30] the binding site of palbociclib to CDK4/6 is the dihydropyridopyrimidine and pyridine, and the piperazine is not an active site. Therefore, ^{99m}Tc-labeled palbociclib and ^{18}F-CDKi both introduced the nuclide through the piperazine. As a consequence, the nuclide introduced through piperazine did not affect the binding affinity. In the present study, we also

https://doi.org/10.1021/acsomega.1c05073
ACS Omega 2021, 6, 32253−32261

conjugated DOTA (1,4,7,10-tetraazacyclododecane-*N*,*N*′,*N*″,*N*‴-tetraacetic acid) through piperazine to enable the complexation of Ga-68. This chelating system allows ^{68}Ga radiolabeling in high efficiency, and the synthesis method is more convenient and time-saving.[31,32]

In the present study, the cell uptake experiment showed that the tracer exhibited high levels of uptake by MCF-7 tumor cells, and the uptake can be sharply inhibited by an excess of palbociclib, indicating that CDK4/6 is the key to the specific uptake of ^{68}Ga-DOTA-palbociclib. Taking into account the interesting findings *in vitro*, a small-animal PET/CT scan was used to further explore the biological properties of the tracer in MCF-7 tumor-bearing mice. From the image, we could find that the radioactivity had significant accumulation in the tumor at 1 h post-injection. Tracer uptake in the tumor decreased by approximately 67% (SUV from 0.63 ± 0.05 to 0.21 ± 0.05) when mice were blocked with an excess of palbociclib, suggesting a CDK4/6-targeting uptake mechanism *in vivo*.

The results of biodistribution data were also in agreement with *in vitro* and PET imaging, and tumor accumulation was very high at 1 and 2 h after injection and significantly decreased when mice received an excess of palbociclib prior to the injection of ^{68}Ga-DOTA-palbociclib. The results of autoradiography and immunofluorescence staining further indicated that ^{68}Ga-DOTA-palbociclib was specifically bound to CDK4 and CDK6 positive tumors. Among the normal organs, the small intestine presented the highest uptake of ^{68}Ga-DOTA-palbociclib, which may explain the relatively high concentration of radioactivity in the abdomen of mice in PET imaging. A high concentration of ^{68}Ga-DOTA-palbociclib was also found in the kidneys, suggesting that the urinary system was the main way to clear ^{68}Ga-DOTA-palbociclib. The uptake in the liver was relatively low over the entire time course of the experiments, which will help improve the diagnosis of hepatic disease in clinical practice. In addition, the distribution in other normal tissues was also relatively low and thus helped to improve the detection of target lesions.

Although palbociclib is the first CDK4/6 inhibitor approved by the FDA and occupied the half part of the CDK4/6 inhibitor clinical application, ribociclib and abemaciclib are also widely used in the clinic. In the present study, the CDK4/6 targeted PET probe was based on palbociclib; therefore, it may be efficient in predicting the response after palbociclib treatment. More precisely, it is not clear that ^{68}Ga-DOTA-palbociclib is also effective in ribociclib and abemaciclib assessment. We will find out the answer in a follow-up study. In the future, we will also explore more CDK4/6 targeted probes based on other inhibitors and will modify the structure of DOTA-palbociclib, improving the characteristics of the tracer to reduce the accumulation in nontarget organs, especially in the small intestine.

CONCLUSIONS

Our results indicate that ^{68}Ga-DOTA-palbociclib could be straightforwardly radiolabeled in a simple and efficient method and exhibited excellent stability and favorable biological performance *in vitro* and *in vivo*. ^{68}Ga-DOTA-palbociclib, as a promising tracer for imaging CDK4/6 with PET, may offer an early assessment of individualized response to CDK4/6 inhibitors in cancer patients.

MATERIALS AND METHODS

DOTA-palbociclib was synthesized by Chinese Peptide Company (Hangzhou, China). NaAc and hydrochloric acid were purchased from Sinopharm Chemical Reagent Co., Ltd. (Shanghai). Acetonitrile (ACN) and trifluoroacetic acid (TFA) were purchased from J&K Science Co., Ltd. (Shanghai, CHN). Instant thin layer chromatography silica gel (ITLC-SG) was obtained from Agilent Technologies (Folsom, CA, USA). A ^{68}Ge-^{68}Ga generator was obtained from Eckert & Ziegler (Berlin, Germany).

The radioactive pharmaceutical was analyzed by radioactive thin layer chromatography (TLC; Raytest mini-GITA) and high-performance liquid chromatography (HPLC), the latter using an Agilent 1200 system equipped with a flow-through γ-detector (Raytest GABI). A ZORBAX 300 SB-C18 (5 μm, 250 × 4.6 mm) column was used for analysis, and the eluting solvents (1 mL/min) used in HPLC were water (solvent A) and acetonitrile (solvent B) with 0.1% trifluoroacetic acid following the gradient: 0−10 min, 25% solvent B.

^{68}Ga Radiolabeling DOTA-Palbociclib. DOTA-palbociclib (20 μg) was dissolved in 640 μL of NaAc (0.5 M) solution. $^{68}GaCl_3$ was eluted from a ^{68}Ge-^{68}Ga generator with 0.1 M HCl, and 2 mL of $^{68}GaCl_3$ (370 MBq) elution was added into the DOTA-palbociclib solution. The final pH of the reaction was adjusted to 4 by HCl, and radiolabeling was performed at 100 °C for 10 min. The product was analyzed by radio-TLC (1 M NH_4Ac/CH_3OH = 1/1 as the mobile phase and on iTLC-SG) and radio-HPLC.

Measurement of the Octanol−Water Partition Coefficient. The lipophilicity of the radiolabeled palbociclib was measured according to our previous study. Approximately 10 μL of ^{68}Ga-DOTA-palbociclib (74 KBq) was mixed with 0.5 mL of water and 0.5 mL of 1-octanol. After stirring in a vortex mixer for 1 min, the organic and water layers were separated by centrifugation. Samples (100 μL) were taken from each layer, and radioactivity was measured in a γ-counter. The experiment was repeated five times.

***In Vitro* and *In Vivo* Stability.** The stability of ^{68}Ga-DOTA-palbociclib was evaluated in phosphate buffer saline (PBS; 0.1 M pH = 7.4) and mouse plasma. ^{68}Ga-DOTA-palbociclib (0.2 mL, 18.5 MBq) was incubated with 0.5 mL of PBS at room temperature for 3 h, and then, the mixture was analyzed by radio-TLC to determine the stability of ^{68}Ga-DOTA-palbociclib. Meanwhile, 0.2 mL of ^{68}Ga-DOTA-palbociclib (18.5 MBq) was added into 0.5 mL of fresh mouse plasma and remained at 37 °C. After 3 h of incubation, 0.5 mL of acetonitrile was added into the plasma to precipitate the protein. The supernatant was analyzed using radio-HPLC to determine the degradation of ^{68}Ga-DOTA-palbociclib. Three normal mice were used to evaluate the *in vivo* stability. ^{68}Ga-DOTA-palbociclib (0.2 mL, 7.4 MBq) was injected into each mouse intravenously. At 5, 30, and 60 min after injection, the mouse was killed by CO_2/O_2 asphyxiation. Blood was obtained by cardiac puncture and collected in a 2 mL microtube. Acetonitrile (200 μL) was added into a 0.5 mL blood sample for the precipitation of protein. The speed of the centrifugation was 10,000 rpm, and the supernatant was indeed analyzed by HPLC with a radioactive detector.

Cell Culture and Animal Models. MCF-7, a human ER +/HER2− breast cancer cell line, was purchased from Cell Bank, Shanghai Institutes for Biological Sciences, Chinese Academy of Sciences. The cells were cultured in an RPMI1640

https://doi.org/10.1021/acsomega.1c05073
ACS Omega 2021, 6, 32253−32261

medium with penicillin (100 μg/mL), streptomycin (100 μg/mL), and 10% fetal bovine serum (FBS) in a humidified 5% CO_2 atmosphere at 37 °C.

All animal studies were approved by the Fudan University Laboratory Animal Ethics Committee and performed according to the ethical principles of animal experimentation. Female BALB/c nude mice (6−8 weeks old) were purchased from Shanghai Lingchang Inst Biotech (Shanghai, CHN) and housed under the conditions of standardized 12 h light/dark cycle, suitable temperature, and ad libitum to feed and water. Five healthy BALB/c mice without a tumor were used for pharmacokinetic measurement. Three days before MCF-7 cell implantation, all tumor-bearing mice were supplemented with an estradiol pellet (0.72 mg, 90 day release, Innovative Research, USA) embedded in the subcutaneous neck area. Twenty-four BALB/c nude mice received subcutaneous injection of MCF-7 cells (2×10^6) in the right shoulder. The mice were studied when the tumor volume reached approximately 320 ± 100 mm^3, and tumor volumes were calculated with the formula (length × $width^2$)/2.

***In Vitro* Uptake.** MCF-7 ER+/HER2− breast cancer cells were seeded in 24-well plates at a density of 2×10^5 per well for 24 h. The next day, cells were incubated with ^{68}Ga-DOTA-palbociclib (0.037 MBq/1 mL per well) at 37 °C for 60 min. When the time is up, cells were first washed three times with phosphate buffer saline (PBS) to remove unbound ^{68}Ga-DOTA-palbociclib. Then, 0.5 mL of NaOH was added, and cell suspensions were collected individually. Finally, radioactivity counts were measured with a γ-counter (SN-697, Shanghai Nuclear Institute Rihuan Photoelectric Instrument Co., Ltd.) at an energy window of 140 ± 19 keV. To determine a specific cell uptake, ^{68}Ga-DOTA-palbociclib was added together with an excess of palbociclib (>1000 molar equivalents, without chelating DOTA) to the MCF-7 cells. After incubation for 1 h, the MCF-7 cell uptake assay was repeated as described above. The experiment was repeated in triplicate. The radioactivity was expressed as counts per minute (CPM).

Pharmacokinetics in Normal Mice. The pharmacokinetics of ^{68}Ga-DOTA-palbociclib was determined in normal mice. Mice (n = 5) were injected via the tail vein with ^{68}Ga-DOTA-palbociclib at a dose of 0.74 MBq/mouse, approximately 200 μL volume. At different time points after injection (1, 3, 5, 7, 10, 15, 30, 60, 120, and 240 min), blood samples were immediately collected by the tail vein using tared capillary tubes. All samples were weighed; radioactivity was measured by a γ-counter and decay-corrected to the time of injection. The pharmacokinetics was analyzed by Prism 5 (Graph-Pad Software) using a two-phase decay least-squares fitting method and expressed as percentage injected dose (%ID)/g.

Small-Animal PET/CT Imaging. For PET/CT imaging, MCF-7 tumor-bearing mice (n = 6) were administered with ^{68}Ga-DOTA-palbociclib (5.55 MBq, 0.2 mL) via tail vein injection. Micro-PET/CT (Inveon, Siemens) scanning was performed at 1 h after radiotracer injection. A blocking study was also performed, and mice (n = 3) were injected with an excess of palbociclib (>1000 molar equivalents) 0.5 h before radiotracer injection. Then, a Micro-PET/CT scan was acquired 1 h later employing the same method. During the scanning, the mice were anesthetized by 1.5% isoflurane gas in oxygen flowing at 0.5 mL/min, and the mice body temperature was maintained by heated air flow under the bed. The PET and CT images were reconstructed using a three-dimensional ordered-subset expectation−maximization (OSEM3D)/maximum algorithm and fused using Inveon Research Workplace software (Siemens Medical Solutions). For data analysis, regions of interest (ROI) were manually drawn around the whole tumor and within quadricep muscles in the fused images. Data were expressed as the mean of standardized uptake value (SUV). The tumor-to-muscle (T/M) ratio was calculated as the ratio of the mean SUV of a tumor to that of contralateral quadricep muscles.

Biodistribution in Tumor-Bearing Mice. For biodistribution studies, MCF-7 tumor-bearing mice were injected with ^{68}Ga-DOTA-palbociclib (0.74 MBq/0.1 mL) via the tail vein. At 1 and 2 h after injection of the radiotracer, the mice (n = 3/per time point) were sacrificed. Tumors and major organs of interest (liver, lung, kidney, spleen, stomach, large intestine, bone, muscle, brain, blood, and heart) were collected, weighed, and measured for their radioactivity by a γ-counter. To confirm the CDK4/6-specific uptake by tumors, a blocking study was performed. In the blocking group, MCF-7 tumor-bearing mice (n = 3) received an injection of an excess of palbociclib (>1000 molar equivalents) 30 min before the injection of ^{68}Ga-DOTA-palbociclib (0.74 MBq/0.1 mL) via the tail vein and sacrificed at 1 h post-injection. The radioactivity uptakes in the organs were expressed as a percentage of the injected radioactive dose per gram of tissue (%ID/g).

Autoradiography and Immunofluorescence. After the γ-counting of tumors from the biodistribution study, tumor tissues were frozen using an optimal cutting temperature (OCT) compound at −80 °C and divided by a cryotome (RM2235, Leica Instruments) into 10 μm-thick slices. Consecutive sections were used for autoradiography and immunofluorescence. The cryosections were placed in an imaging plate for autoradiography. After a 3 h exposure, the plates were scanned with a Fuji Analyzer BAS-5000 (Fuji, Tokyo, Japan). Phosphor imaging plates were read by a Typhoon 9500 IP plate reader (GE Healthcare Life Sciences).

For immunofluorescence techniques, the adjacent slides were fixed with 4% paraformaldehyde in PBS and stained with anti-CDK4 (ab68266, Abcam) and anti-CDK6 antibodies (ab68266, Abcam). The sections were placed in a humidified chamber and incubated overnight at 4 °C. Sections were washed with PBS, and Alexa Fluor-conjugated secondary antibodies (Thermo Fisher Scientific) were incubated for 50 min at room temperature and shielded from direct light. Slides were counterstained with DAPI and mounted in medium for fluorescence (Invitrogen). Sections were observed under an inverted fluorescence microscope (NIKON ECLIPSE CI-S), and images were collected.

Statistical Analysis. All data were expressed as mean ± standard deviation (SD). Differences between cohorts were analyzed with one-way analysis of variance or t test using GraphPad Prism (version 5.01, San Diego, California USA). Results with a P-value less than 0.05 were considered statistically significant.

AUTHOR INFORMATION

Corresponding Authors

Shaoli Song − *Department of Nuclear Medicine, Fudan University Shanghai Cancer Center, Shanghai 200032, China; Department of Oncology, Shanghai Medical College and Shanghai Institute of Medical Imaging, Fudan University, Shanghai 200032, China; Shanghai Engineering Research Center of Molecular Imaging Probes, Shanghai*

https://doi.org/10.1021/acsomega.1c05073
ACS Omega 2021, 6, 32253−32261

200032, China; Department of Nuclear Medicine, Shanghai Proton and Heavy Ion Center, Fudan University Cancer Hospital, Shanghai 201315, China; Phone: +86-21-64175590-86908; Email: shaoli-song@163.com; Fax: +86-21-54520250

Xiaoping Xu − *Department of Nuclear Medicine, Fudan University Shanghai Cancer Center, Shanghai 200032, China; Department of Oncology, Shanghai Medical College, Fudan University, Shanghai 200032, China; Shanghai Engineering Research Center of Molecular Imaging Probes, Shanghai 200032, China*; Email: xxp0012@ustc.edu

Zhongyi Yang − *Department of Nuclear Medicine, Fudan University Shanghai Cancer Center, Shanghai 200032, China; Department of Oncology, Shanghai Medical College, Fudan University, Shanghai 200032, China; Shanghai Engineering Research Center of Molecular Imaging Probes, Shanghai 200032, China*; orcid.org/0000-0001-6195-9942; Email: yangzhongyi21@163.com

Authors

Cheng Liu − *Department of Nuclear Medicine, Fudan University Shanghai Cancer Center, Shanghai 200032, China; Department of Oncology, Shanghai Medical College and Shanghai Institute of Medical Imaging, Fudan University, Shanghai 200032, China; Shanghai Engineering Research Center of Molecular Imaging Probes, Shanghai 200032, China; Department of Nuclear Medicine, Shanghai Proton and Heavy Ion Center, Fudan University Cancer Hospital, Shanghai 201315, China*

Ziyi Yang − *Department of Nuclear Medicine, Fudan University Shanghai Cancer Center, Shanghai 200032, China; Department of Oncology, Shanghai Medical College, Fudan University, Shanghai 200032, China; Shanghai Engineering Research Center of Molecular Imaging Probes, Shanghai 200032, China*

Mingyu Liu − *Department of Nuclear Medicine, Fudan University Shanghai Cancer Center, Shanghai 200032, China; Department of Oncology, Shanghai Medical College, Fudan University, Shanghai 200032, China; Shanghai Engineering Research Center of Molecular Imaging Probes, Shanghai 200032, China; Department of Nuclear Medicine, Shanghai Proton and Heavy Ion Center, Fudan University Cancer Hospital, Shanghai 201315, China*

Xiangwei Wang − *Department of Nuclear Medicine, Fudan University Shanghai Cancer Center, Shanghai 200032, China; Department of Oncology, Shanghai Medical College, Fudan University, Shanghai 200032, China; Shanghai Engineering Research Center of Molecular Imaging Probes, Shanghai 200032, China*

Complete contact information is available at: https://pubs.acs.org/10.1021/acsomega.1c05073

Author Contributions

#C.L. and Z.Y. contributed equally to this work. C.L., Z.Y., and X.X. participated in the experimental and data analysis. C.L. and X.X. wrote the manuscript. C.L., Z.Y., M.L., and X.W. were involved in cell studies and animal imaging and dealt with the tumors. X.X., S.S., and Z.Y. helped in polishing the articles. C.L., X.X., and Z.Y. designed and controlled the quality of the study. All authors have reviewed the manuscript.

Funding

This study was funded by the National Key Research and Development Program of China (2020YFA0909003), Shanghai Sailing Program (20YF1408500), Science and Technology Development Fund of Shanghai Pudong New Area (PKJ2020-Y54), Shanghai Committee of Science and Technology Fund (19ZR1411300), and Shanghai Municipal Health Commission (202040269).

Notes

The authors declare no competing financial interest.

■ ACKNOWLEDGMENTS

We wish to thank Jianping Zhang and Simin He for excellent technical assistance.

■ REFERENCES

(1) Jackson, S. P.; Helleday, T. DNA REPAIR. Drugging DNA repair. *Science (New York, N.Y.)* **2016**, *352*, 1178−1179.

(2) Hanahan, D.; Weinberg, R. A. Hallmarks of cancer: the next generation. *Cell* **2011**, *144*, 646−674.

(3) Rubin, S. M.; Sage, J.; Skotheim, J. M. Integrating Old and New Paradigms of G1/S Control. *Mol. Cell* **2020**, *80*, 183−192.

(4) Wenzel, E. S.; Singh, A. T. K. Cell-cycle Checkpoints and Aneuploidy on the Path to Cancer. *In vivo (Athens, Greece)* **2018**, *32*, 1−5.

(5) Skotheim, J. M.; Di Talia, S.; Siggia, E. D.; Cross, F. R. Positive feedback of G1 cyclins ensures coherent cell cycle entry. *Nature* **2008**, *454*, 291−296.

(6) Di Sante, G.; Pagé, J.; Jiao, X.; Nawab, O.; Cristofanilli, M.; Skordalakes, E.; Pestell, R. G. Recent advances with cyclin-dependent kinase inhibitors: therapeutic agents for breast cancer and their role in immuno-oncology. *Expert review of anticancer therapy* **2019**, *19*, 569−587.

(7) Rubio, C.; Martínez-Fernández, M.; Segovia, C.; Lodewijk, I.; Suarez-Cabrera, C.; Segrelles, C.; López-Calderón, F.; Munera-Maravilla, E.; Santos, M.; Bernardini, A.; García-Escudero, R.; Lorz, C.; Gómez-Rodriguez, M. J.; de Velasco, G.; Otero, I.; Villacampa, F.; Guerrero-Ramos, F.; Ruiz, S.; de la Rosa, F.; Domínguez-Rodríguez, S.; Real, F. X.; Malats, N.; Castellano, D.; Dueñas, M.; Paramio, J. M. CDK4/6 Inhibitor as a Novel Therapeutic Approach for Advanced Bladder Cancer Independently of RB1 Status. *Clin Cancer Res* **2019**, *25*, 390−402.

(8) Finn, R. S.; Martin, M.; Rugo, H. S.; Jones, S.; Im, S. A.; Gelmon, K.; Harbeck, N.; Lipatov, O. N.; Walshe, J. M.; Moulder, S.; Gauthier, E.; Lu, D. R.; Randolph, S.; Diéras, V.; Slamon, D. J. Palbociclib and Letrozole in Advanced Breast Cancer. *The New England journal of medicine* **2016**, *375*, 1925−1936.

(9) Slamon, D. J.; Neven, P.; Chia, S.; Fasching, P. A.; De Laurentiis, M.; Im, S. A.; Petrakova, K.; Bianchi, G. V.; Esteva, F. J.; Martín, M.; Nusch, A.; Sonke, G. S.; De la Cruz-Merino, L.; Beck, J. T.; Pivot, X.; Vidam, G.; Wang, Y.; Rodriguez Lorenc, K.; Miller, M.; Taran, T.; Jerusalem, G. Phase III Randomized Study of Ribociclib and Fulvestrant in Hormone Receptor-Positive, Human Epidermal Growth Factor Receptor 2-Negative Advanced Breast Cancer: MONALEESA-3. *Journal of clinical oncology : official journal of the American Society of Clinical Oncology* **2018**, *36*, 2465−2472.

(10) Sledge, G. W., Jr.; Toi, M.; Neven, P.; Sohn, J.; Inoue, K.; Pivot, X.; Burdaeva, O.; Okera, M.; Masuda, N.; Kaufman, P. A.; Koh, H.; Grischke, E. M.; Conte, P.; Lu, Y.; Barriga, S.; Hurt, K.; Frenzel, M.; Johnston, S.; Llombart-Cussac, A. The Effect of Abemaciclib Plus Fulvestrant on Overall Survival in Hormone Receptor-Positive, ERBB2-Negative Breast Cancer That Progressed on Endocrine Therapy-MONARCH 2: A Randomized Clinical Trial. *JAMA Oncol* **2020**, *6*, 116−124.

(11) Hortobagyi, G. N.; Stemmer, S. M.; Burris, H. A.; Yap, Y. S.; Sonke, G. S.; Paluch-Shimon, S.; Campone, M.; Blackwell, K. L.; André, F.; Winer, E. P.; Janni, W.; Verma, S.; Conte, P.; Arteaga, C. L.; Cameron, D. A.; Petrakova, K.; Hart, L. L.; Villanueva, C.; Chan, A.; Jakobsen, E.; Nusch, A.; Burdaeva, O.; Grischke, E. M.; Alba, E.; Wist, E.; Marschner, N.; Favret, A. M.; Yardley, D.; Bachelot, T.;

Tseng, L. M.; Blau, S.; Xuan, F.; Souami, F.; Miller, M.; Germa, C.; Hirawat, S.; O'Shaughnessy, J. Ribociclib as First-Line Therapy for HR-Positive, Advanced Breast Cancer. *N. Engl. J. Med.* **2016**, *375*, 1738−1748.
(12) Zhang, J.; Wang, Q.; Wang, Q.; Cao, J.; Sun, J.; Zhu, Z. Mechanisms of resistance to estrogen receptor modulators in ER +/HER2- advanced breast cancer. *Cell. Mol. Life Sci.* **2020**, *77*, 559−572.
(13) Loibl, S.; Turner, N. C.; Ro, J.; Cristofanilli, M.; Iwata, H.; Im, S. A.; Masuda, N.; Loi, S.; André, F.; Harbeck, N.; Verma, S.; Folkerd, E.; Puyana Theall, K.; Hoffman, J.; Zhang, K.; Bartlett, C. H.; Dowsett, M. Palbociclib Combined with Fulvestrant in Premenopausal Women with Advanced Breast Cancer and Prior Progression on Endocrine Therapy: PALOMA-3 Results. *The oncologist* **2017**, *22*, 1028−1038.
(14) Decristoforo, C.; Pickett, R. D.; Verbruggen, A. Feasibility and availability of ^{68}Ga-labelled peptides. *Eur. J. Nucl. Med. Mol. Imaging* **2012**, *39 Suppl 1*, S31−S40.
(15) Kumar, K. The Current Status of the Production and Supply of Gallium-68. *Cancer biotherapy & radiopharmaceuticals* **2020**, *35*, 163−166.
(16) Kratochwil, C.; Flechsig, P.; Lindner, T.; Abderrahim, L.; Altmann, A.; Mier, W.; Adeberg, S.; Rathke, H.; Röhrich, M.; Winter, H.; Plinkert, P. K.; Marme, F.; Lang, M.; Kauczor, H. U.; Jäger, D.; Debus, J.; Haberkorn, U.; Giesel, F. L. (68)Ga-FAPI PET/CT: Tracer Uptake in 28 Different Kinds of Cancer. *J Nucl Med* **2019**, *60*, 801−805.
(17) Liu, C.; Li, T.; Tao, Z.; Cao, J.; Wang, L.; Zhang, J.; Wang, B.; Hu, X. Clinical Outcomes of 130 Patients with Hormone Receptor-Positive and Human Epidermal Growth Factor Receptor 2-Negative Metastatic Breast Cancer Treated with Palbociclib plus Endocrine Therapy and Subsequent Therapy: A Real-World Single-Center Retrospective Study in China. *Medical science monitor : international medical journal of experimental and clinical research* **2020**, *26*, No. e927187.
(18) Garrido-Castro, A. C.; Goel, S. CDK4/6 Inhibition in Breast Cancer: Mechanisms of Response and Treatment Failure. *Curr. Breast Cancer Rep.* **2017**, *9*, 26−33.
(19) Huober, J.; Schneeweiss, A.; Hartkopf, A. D.; Müller, V.; Lux, M. P.; Janni, W.; Ettl, J.; Belleville, E.; Thill, M.; Fasching, P. A.; Kolberg, H. C.; Schulmeyer, C. E.; Welslau, M.; Overkamp, F.; Tesch, H.; Fehm, T. N.; Lüftner, D.; Schütz, F.; Wöckel, A. Update Breast Cancer 2020 Part 3 - Early Breast Cancer. *Geburtshilfe Frauenheilkd* **2020**, *80*, 1105−1114.
(20) Knudsen, E. S.; Witkiewicz, A. K. The Strange Case of CDK4/6 Inhibitors: Mechanisms, Resistance, and Combination Strategies. *Trends Cancer* **2017**, *3*, 39−55.
(21) Fang, H.; Huang, D.; Yang, F.; Guan, X. Potential biomarkers of CDK4/6 inhibitors in hormone receptor-positive advanced breast cancer. *Breast cancer research and treatment* **2018**, *168*, 287−297.
(22) McCartney, A.; Migliaccio, I.; Bonechi, M.; Biagioni, C.; Romagnoli, D.; De Luca, F.; Galardi, F.; Risi, E.; De Santo, I.; Benelli, M.; Malorni, L.; Di Leo, A. Mechanisms of Resistance to CDK4/6 Inhibitors: Potential Implications and Biomarkers for Clinical Practice. *Front. Oncol.* **2019**, *9*, 666.
(23) He, M.; Liu, C.; Shi, Q.; Sun, Y.; Zhang, Y.; Xu, X.; Yuan, H.; Zhang, Y.; Liu, Y.; Liu, G.; Di, G.; Yang, Z.; Wang, Z.; Shao, Z. The Predictive Value of Early Changes in (18) F-Fluoroestradiol Positron Emission Tomography/Computed Tomography During Fulvestrant 500 mg Therapy in Patients with Estrogen Receptor-Positive Metastatic Breast Cancer. *The oncologist* **2020**, *25*, 927−936.
(24) Elmi, A.; Makvandi, M.; Weng, C. C.; Hou, C.; Clark, A. S.; Mach, R. H.; Mankoff, D. A. Cell-Proliferation Imaging for Monitoring Response to CDK4/6 Inhibition Combined with Endocrine-Therapy in Breast Cancer: Comparison of [(18)F]FLT and [(18)F]ISO-1 PET/CT. *Clin Cancer Res* **2019**, *25*, 3063−3073.
(25) Koehler, L.; Graf, F.; Bergmann, R.; Steinbach, J.; Pietzsch, J.; Wuest, F. Radiosynthesis and radiopharmacological evaluation of cyclin-dependent kinase 4 (Cdk4) inhibitors. *Eur. J. Med. Chem.* **2010**, *45*, 727−737.
(26) Song, X.; Gan, Q.; Zhang, X.; Zhang, J. Synthesis and Biological Evaluation of Novel (99m)Tc-Labeled Palbociclib Derivatives Targeting Cyclin-Dependent Kinase 4/6 (CDK4/6) as Potential Cancer Imaging Agents. *Mol. Pharmaceutics* **2019**, *16*, 4213−4222.
(27) Gan, Q.; Song, X.; Zhang, X.; Zhang, J. Preparation and evaluation of (99m)Tc-labeled HYNIC-palbociclib analogs for cyclin-dependent kinase 4/6-positive tumor imaging. *Eur. J. Med. Chem.* **2020**, *188*, 112032.
(28) Ramos, N.; Baquero-Buitrago, J.; Ben Youss Gironda, Z.; Wadghiri, Y. Z.; Reiner, T.; Boada, F. E.; Carlucci, G. Noninvasive PET Imaging of CDK4/6 Activation in Breast Cancer. *J Nucl Med* **2020**, *61*, 437−442.
(29) Rahmim, A.; Zaidi, H. PET versus SPECT: strengths, limitations and challenges. *Nucl Med Commun* **2008**, *29*, 193−207.
(30) Zhao, B.; Burgess, K. PROTACs suppression of CDK4/6, crucial kinases for cell cycle regulation in cancer. *Chem. Commun.* **2019**, *55*, 2704−2707.
(31) Vaz, S. C.; Oliveira, F.; Herrmann, K.; Veit-Haibach, P. Nuclear medicine and molecular imaging advances in the 21st century. *The British journal of radiology* **2020**, *93*, 20200095.
(32) Martiniova, L.; Palatis, L.; Etchebehere, E.; Ravizzini, G. Gallium-68 in Medical Imaging. *Curr. Radiopharm.* **2016**, *9*, 187−207.

https://doi.org/10.1021/acsomega.1c05073
ACS Omega 2021, 6, 32253−32261